THE ASTROPHYSICAL JOURNAL, 367:L1–L4, 1991 January 20

A TECHNIQUE FOR USING RADIO JETS AS EXTENDED GRAVITATIONAL LENSING PROBES

PHILIPP P. KRONBERG[1,2] AND CHARLES C. DYER
Department of Astronomy and Scarborough College, University of Toronto, Toronto (West Hill), Ontario, Canada M1C 1A4
AND
E. MARGARET BURBIDGE[3] AND VESA T. JUNKKARINEN[3]
Center for Astrophysics and Space Sciences, University of California, San Diego, CASS C-011, La Jolla, CA 92093
Received 1990 July 30; accepted 1990 November 6

ABSTRACT

We propose a new and potentially powerful method of measuring the mass of a galaxy (or dark matter concentration) which lies close in position to a background *polarized* radio jet. Using the fact that the polarization angle is not changed by lensing, we define an "alignment-breaking parameter" η_G, which we show to be a sensitive indicator of gravitational distortion. The method remains sensitive over a wide redshift range of the gravitational lens. We apply our technique to the analysis of polarimetric observations of the jet of 3C 9 at $z = 2.012$, combined with a newly discovered 20.3 mag foreground galaxy at $z = 0.2538$ to "weigh" the galaxy and obtain an approximate upper limit to the mass-to-light ratio.

Subject headings: dark matter — gravitational lenses — polarization — quasars — radio sources: galaxies

1. INTRODUCTION

Recent specification of the polarization structure and Faraday rotation within radio "jets" in QSOs raises a new possibility which we discuss in this *Letter*, namely, the question of whether the polarization properties of extended radio jets can be used to probe for gravitational bending of photon paths due to intervening galaxy systems.

A review of the known optically lensed QSOs and their interpretation has, by and large, not yet led to unambiguous derivations of the masses or mass distributions in lensing systems (cf. Turner 1987). The first, and best studied, example is 0957+561 (Walsh, Carswell, & Weymann 1979), whose optical and radio morphology have since been analyzed in great detail (Greenfield, Roberts, & Burke 1985; Gorenstein et al. 1988).

Extended radio quasars have the advantage that, unlike stellar-like objects which probe the intervenor potential at a few discrete points, they provide a continuous image which, in principle, can furnish more information about the full shape of the intervening gravitational potential. Their great disadvantage is that there is no standard intrinsic morphological shape, whose gravitationally distorted image can be unambiguously compared with intervenor potential distributions. An exception, however, has been the recently discovered, strongly lensed quasar MG 1131+0456 (Hewitt et al. 1988) whose Einstein ring could be recognized and inverted to give a plausible galaxy-like, elliptical gravitational potential for the lensing system (Kochanek et al. 1989).

In this *Letter* we propose a technique involving the intrinsic polarization structure, which makes it possible to detect the gravitational distortion of radio source features independent of other intrinsic, nongravitational causes of distortion. Our method should also work for "mildly" lensed sources (as opposed to "strongly" lensed ones—those which are close to the Einstein ring), and hence could prove to be a more sensitive probe of intervening potentials in the universe.

To apply our method to a real system, we present radio and optical observations of 3C 9, a radio jet QSO at $z = 2.012$, for which we have also discovered a nearby foreground galaxy. We briefly describe this galaxy, which lies about 10″ away from the 3C 9 jet, and apply our new gravitational lens probe technique to place an upper limit on its total mass.

2. POLARIZED RADIO JETS AS EXTENDED LINEAR-EQUIVALENT PROBES OF COSMIC GRAVITATIONAL LENSES

At least for small gravitational distortions, the local plane of polarization does *not* undergo a rotation due to gravitational effects. Of course, the polarization distribution at a given radio frequency can be Faraday-rotated by the magnetoionic component of any intervening system. However, the amount of Faraday rotation at each image point can in principle be determined by multifrequency mapping of the polarized extended emission, and the polarization directions derotated to obtain the intrinsic polarization distribution.

If the projected magnetic field direction (at 90° to the intrinsic polarization direction, χ_0) is aligned to the local "ridge" direction (ψ) of the jet, any gravitational bending will alter only the *difference* between the intrinsic polarization angle and the *local* projected jet angle. We shall define this difference, η_G, as the *gravitational alignment-breaking angle*. It can be expressed as

$$\eta_G(\theta) = \psi(\theta) - [\chi_0(\theta) + 90°] + \kappa(\theta) , \tag{1}$$

where κ is a source physics–dependent angle which allows for a source-intrinsic variation of η_G, where θ defines a contiguous family of positions in space, e.g., along the ridge line of a jet (they need not be colinear). The value of η_G will vary if the strength of the gravitational bending varies along the jet (assuming κ to be constant, or independently derivable). We

[1] Visiting Humboldt Prizeholder at the Max-Planck-Institut für Radioastronomie, Bonn, Germany.

[2] Postal address: Max-Planck-Institut für Radioastronomie, Auf dem Hügel 69, D-5300 Bonn 1, Germany.

[3] Visiting Astronomer, Kitt Peak National Observatory, which is operated by the Association of Universities for Research in Astronomy, Inc., under contract with the National Science Foundation.

will use δ as the coordinate transverse to the jet direction on the sky.

Polarization maps of radio source jets reveal a generally high degree of alignment between the intrinsic (Faraday-derotated) position angle and the local direction of the radio jet (see, e.g., Perley, Bridle, & Willis 1984; Bridle, Perley, & Henriksen 1986; and Killeen, Bicknell, & Ekers 1986). In particular, the intrinsic maximum E-vector orientation in strong jets is typically perpendicular to ψ, and if it does change, it is usually a 90° flip—which would be reflected in $\kappa(\theta)$ in equation (1). Confidence in the jet-intrinsic magnetic field geometry is beginning to improve through computational MHD modeling of radio jets (cf. Clarke, Norman, & Burns 1989). To the extent that we can be reasonably confident of the predictability of the intrinsic $\chi_0(\theta)$ distribution, the method we are proposing converts a bent jet into an effectively linear space probe for gravitational bending. The typical extent of quasar jets is tens of kiloparsecs. This is *comparable to the characteristic size of a typical mass intervenor*, so that quasar jet probes provide a spatially contiguous set of "images" which are well suited for obtaining the differential gravitational distortion across an intervening gravitational potential. With sufficiently good data, the total mass, and mass scale in a lens halo could be determined.

We now consider the simple case of a ray passing close to a spherical deflector, for which we will follow the discussion of Dyer & Roeder (1981). For a given impact parameter, h, the Einstein bending angle is $4\tilde{m}(h)/h$, where $\tilde{m}(h)$ is the cylindrical mass, or projected mass defined by radius h. This requires that the projected density of the lens be less divergent than $1/h$ as $h \to 0$. Defining h_c to be the classical, "undeviated," impact parameter, the allowed rays are the solutions of the equation

$$h = h_c + D\tilde{m}(h)/h \,, \tag{2}$$

where $D = 4s_{lo}s_{le}/s_{oe}$ is the distance factor; s_{lo} and s_{le} are the angular size distances from the lens to the observer and the emitter, respectively; and s_{oe} is the angular size distance from the observer to the emitter. For the purposes of this discussion, we will consider the case of a truncated King (1972) distribution, whose radial density is $\rho = \rho_o(1 + x^2)^{-3/2}$, where x is the radius in units of a core radius, a_G, and we shall assume a cutoff radius of x_G in units of a_G. The function $\tilde{m}(h)$ is then given by

$$\frac{\tilde{m}}{m_G} = \left\{\sqrt{x_G^2+1}\,\ln\left[\frac{\sqrt{k^2+1}(x_G+\sqrt{x_G^2+1})}{(\sqrt{x_G^2+1}+\sqrt{x_G^2+k^2})}\right] + \sqrt{x_G^2-k^2} - x_G\right\} \times [\sqrt{x_G^2+1}\,\ln(x_G+\sqrt{x_G^2+1}) - x_G]^{-1} \,, \tag{3}$$

where m_G is the total mass of the lens, and k is the cylindrical radius, h, in units of a_G. Since we are mainly interested in the displaced classical jet, it is simple to use equation (2) with equation (3) to find the values of h for each h_c by iteration. In this way a point-to-point displacement map of the classical "straight" jet to its new shape can be obtained.

If the lens mass distribution is sufficiently centrally condensed, the lens is capable of producing multiple images of those parts of the jet that lie within a particular distance of the lens center, as discussed by Dyer & Roeder (1980). In the prototype case considered here, this requires a total lens mass in excess of $40 \times 10^{11}\ M_\odot$, although the "trigger-level" mass for multiple imaging depends on the mass distribution (see below). In better aligned cases, a smaller mass would be sufficient to cause multiple imaging of the jet.

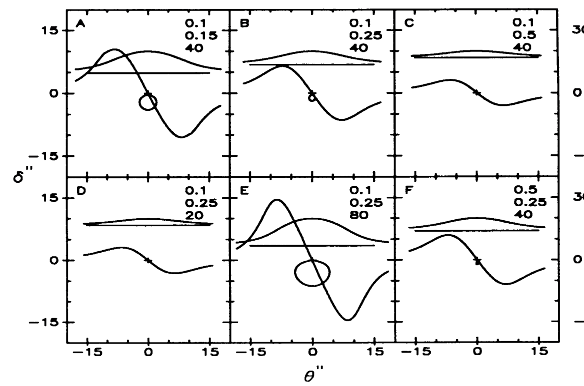

FIG. 1.—Six sample theoretical models of the jet distortion are shown. The lens galaxy, represented by the plus sign, is at the origin of the sky coordinates. The value of δ is in arcseconds, η_G is in degrees, and θ is the angular distance along the jet measured, in this case, from the normal to the lens center. The straight line represents the unlensed classical, straight jet, as it would appear on the sky. The curve above this straight jet represents the apparent jet after the lensing effect has been added. The quasi-sinusoidal curve passing through the lens shows the *gravitational alignment-breaking angle*, η_G, along the jet, based on the scale in degrees at the right of the figure. Each frame is labeled with (1) q_0, (2) the lens redshift, and (3) the lens mass in units of $10^{11}\ M_\odot$. Panel sequences of interest are [(*a*), (*b*), (*c*)] for variation of z, [(*d*), (*b*), (*e*)] for variation of lens mass, [(*b*), (*f*)] for variation of q_0.

Figure 1 illustrates schematically the variation of η_G versus θ for a hypothetical jet at $z = 2$ due to gravitational distortion by an intervening galaxy at different redshifts for some sample intervenor masses (using the King mass distribution model). It is seen that, whereas the angular displacement of a point on the undistorted locus (a straight line in this case) is small and difficult to disentangle from intrinsic jet bending, the detectability of a real signal in η_G is substantially higher than that of simple jet bending.

Figure 1 shows in particular that gravitational bending would be most sensitively detected where $d\eta_G/d\theta$ is greatest. Furthermore, if the intervenor can be seen, e.g., optically, the approximate *locations* of the two maxima of $d\eta_G/d\theta$ are predetermined. This fact further increases the power of the method, in that any residual variations of $\kappa(\theta)$ [which are independent of variations $\eta_G(\theta)$] should be easier to separate from the gravitational bending effects. In this way the gravitational bending effect on η_G versus θ can be expected to have a characteristic "signature" variation versus θ. For larger intervenor masses/small impact parameters, secondary and tertiary images of a portion of the jet are produced, which form a closed loop on the opposite side of the lens. The two components of this loop each contain a "copy" of the polarization structure of the multiply imaged portion of the jet. This provides further constraints on the lensing system's mass distribution. The case of multiply imaged jets will be discussed in detail in a subsequent paper.

While the effect is, from Figure 1, clearly quite sensitive to the mass of the intervenor, it is relatively insensitive to the choice of the deceleration parameter, q_o. Of particular note is the fact that the effect is enhanced when the lens is at reasonably small redshifts, say 0.15–0.25, compared to its level at larger lens redshifts, such as 0.5. This is a useful property for a number of reasons, including the fact that the lensing object is accessible to detailed observation at more modest redshifts.

As a demonstration of the method, we describe the analysis of radio and optical observations of the QSO 3C 9, which has a polarized radio jet, a redshift of 2.012, and an intermediate redshift galaxy about 10″ from the apparent jet.

3. THE OBSERVATIONS AND RESULTS

3.1. *Radio Observations*

The quasar 3C 9 was observed in the Stokes parameters I, Q, and U with the NRAO VLA[4] at 1370, 1465, 1652, and 4885 MHz in 1980 January and again in 1982 February. The 1980 observations were made with 20 antennas, and the 1982 observations used the full A-array configuration with 27 antennas. The maps were similar, except that the later observations used the full VLA resolution—at 1370, 1652, and 4885 MHz. This combination of antenna configuration and frequencies was chosen so that a reliable Faraday rotation map could be generated to produce a $\chi_0(\theta)$ distribution at the highest possible resolution—1″.4 common to the three frequencies used. The calibrators were 3C 286, 0007+171, and 3C 138. Polarization maps were produced at each frequency so that the intrinsic polarization angle could be determined along 3C 9's radio jet, to obtain an estimate of η_G.

3.2. *Optical Observations*

One of the four red plates of the Palomar Observatory Sky Survey that cover the region of the QSO 3C 9 shows a very faint object near 3C 9. We therefore decided to obtain deep exposure, direct images of the field around 3C 9, to examine the very faint nearby object and to see whether other objects, too faint to appear on the POSS, might be present. Two plates, numbers 3259 and 3260, were obtained at the prime focus of the 4 m telescope at Kitt Peak on 1979 October 25. The exposures were each 60 minutes on baked IIIa-J emulsion through a GG 385 filter.

The only object seen near 3C 9 was the faint red "star" seen on the POSS. Scans of the profile of this object and comparison with stars in the field showed it to be slightly extended, and thus to be possibly a faint compact galaxy. Figure 2 (Plate L1) shows an overlay of the total intensity and linear polarization at 4885 MHz, superposed on the optical field from the KPNO 4 m plate, after using standard astrometric techniques to determine the position of the optical QSO. The 4 m plates show no additional objects near 3C 9, down to $m \sim 22.5$.

With the lens-grism CCD spectrograph on the Shane 3 m telescope at Lick Observatory, we were able to obtain spectra of the faint object. Four spectra were obtained on 1985 October 16 and 17, in clear weather with good seeing. A 420 lines mm^{-1} grism was used, with a 3″ slit, and the integrations were, respectively, 60, 45, 60, and 60 minutes. The reduced data, summed, are shown in Figure 3. Four narrow emission lines were seen: [O II] (3727), Hβ, [O III](5007), and Hα at redshifts, respectively, of 0.2549, 0.2538, 0.2539, and 0.2528. They clearly show that the object is a faint emission-line galaxy. The wavelengths are heliocentric measured values not corrected to vacuum wavelengths. The mean redshift is 0.2538 ± 0.001.

No attempt was made to observe the galaxy through a large aperture for accurate photometry; thus we have applied a small correction for light excluded by the 3″ sit and derive an apparent V magnitude $m = 20.3 \pm 0.3$. Using the observed

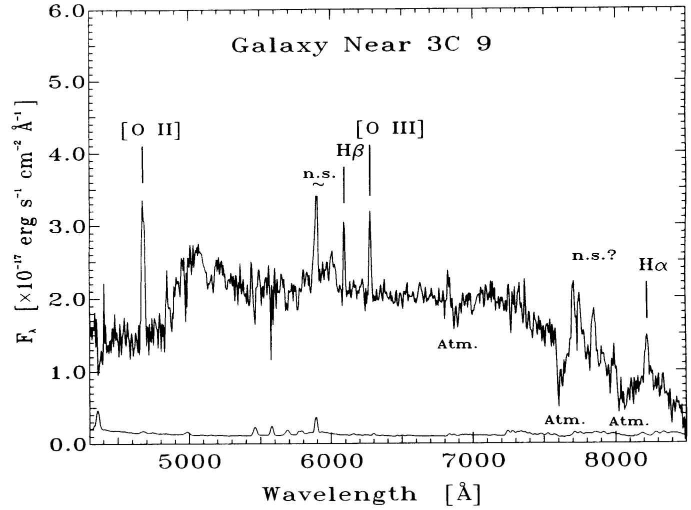

FIG. 3.—Optical spectrum of the galaxy near 3C 9 at a resolution of 20 Å FWHM, displayed as flux per unit wavelength vs. air wavelength. The expected positions of emission features at z(galaxy) = 0.2538 are marked. Wavelengths affected by poor subtraction of night sky lines are marked "n.s." and absorption features in Earth's atmosphere are marked "atm." The 1 σ error is shown below the spectrum.

spectral energy distribution for a K-correction, we estimate the absolute visual magnitude $M_V = -20.1$ for $H_0 = 75$ km s^{-1} Mpc^{-1}, $q_0 = 0.1$.

A higher resolution, higher S/N spectrum of 3C 9 itself was obtained with the Lick UV Schmidt CCD spectrograph, in the region of Lyman-α, to check whether the Mg II λ2800 absorption doublet might appear, due to an extended gaseous envelope around the compact galaxy. Unfortunately, the Mg II doublet falls in the Lyα forest of 3C 9; there are absorptions very near the expected position, but they do not coincide with Mg II at $z = 0.2538$.

3.3. *Comparison of Measured η_G Values for the 3C 9 Jet with Gravitational Lensing Calculations*

We have measured η_G at seven positions along the 3C 9 jet, with the assumption that $\kappa(\theta) = 0$ or the entire range of positions with sufficient polarized signal at all three frequencies. Rotation measure variations were small and close to the integrated value of -22 ± 1 rad/m^{-2} (Simard-Normandin, Kronberg, & Button 1981). The data are shown in Figure 4, compared with model η_G curves for three different total masses for the $z = 0.2538$ galaxy in Figure 2.

Although the uncertainty in the measured points is high, they happen to lie at a favorable position along the 3C 9 jet—just where $d\eta_G/d\theta$ is greatest. For $H_0 = 75$, $q_0 = 0.1$, a core radius of 2 kpc, and cutoff radius of 30 kpc (8″.6), the η values are consistent with a galaxy mass in the range 10–40 $\times 10^{11}$ solar masses. It should be emphasized that the η_G data for 3C 9 in Figure 4 are crude and have a large internal scatter; hence, this mass value is tentative. It nonetheless serves to demonstrate the method and suggests a mass for the lensing galaxy. Our result implies a mass-to-light ratio in solar units (within 30 kpc of the galaxy's nucleus) in the range 100–400. If this is correct, then the lensing galaxy's M/L would be higher than expected for similar galaxies, previous estimates (to a radius of 30 kpc) being in the range 20–80.

An independent and definitive upper limit can be established by the absence of the closed-loop multiple image structure

[4] The National Radio Astronomy Observatory is operated by the Associated Universities under contract with the National Science Foundation.

1991ApJ...367L...1K

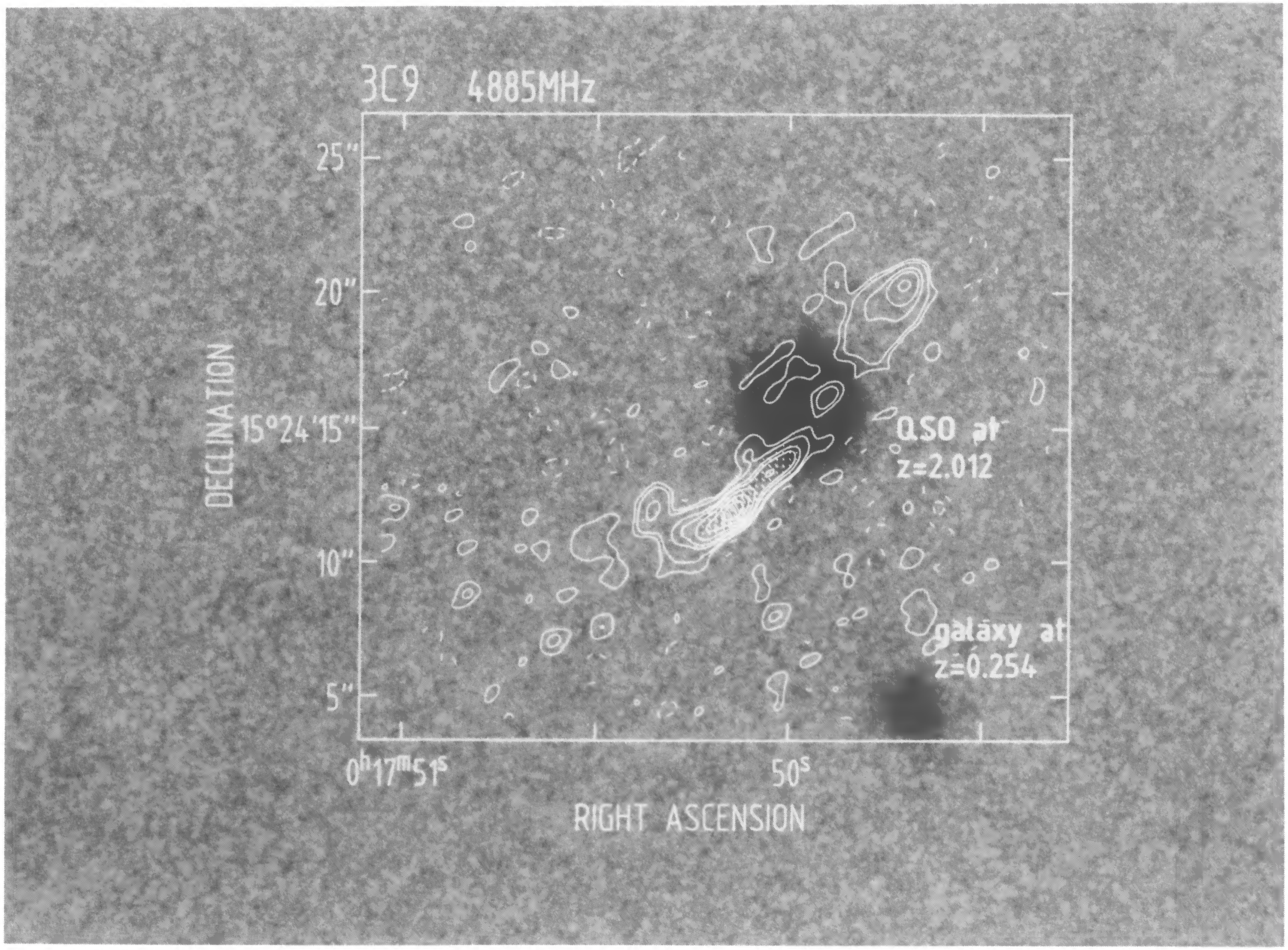

FIG. 2.—Radio-optical superposition for 3C 9. The radio map has a resolution of 0".96 by 0".56, elongated in p.a. 139°. Radio surface brightness contours are as shown at −2, −1, 1, 2, 6, 10, 20, 40, and 70% of the peak surface brightness, which is 142 mJy beam^{-1}. The optical position of the QSO is $00^h17^m49^s.944$, +15°24'16".21 (from Murray, Tucker, & Clements 1971).

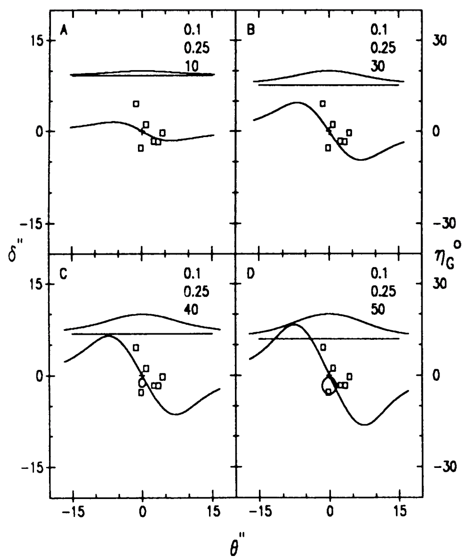

FIG. 4.—The measured values of η_G at several positions along the jet of 3C 9 compared with superimposed model η_G curves for King mass models of the $z = 0.2538$ galaxy in Fig. 2. The quasar lies at the position $\theta \approx +7''.5$.

which sets in at about 40×10^{11} solar masses and above, for the mass distribution parameter used in Figure 4. If we reduce the core radius from a (relatively "soft") 2 kpc to 0.2 kpc, the observed absence of a secondary/tertiary image loop in the radio map limits the total mass to 15×10^{11} $M_\odot$ (an M/L upper limit of ~ 166). This limit is also consistent with the (independently) estimated mass range from the η_G curves in Figure 4.

4. SUMMARY

The *gravitational alignment-breaking angle*, η_G, of a polarized radio jet provides a potentially powerful probe of intervening galaxy-scale mass concentrations in the universe. In contrast to optical quasars, it provides us with a quasi-linear probe, whose dimensions are comparable to, or greater than, those of the gravitational lens itself.

Although the method is subject to possible uncertainties in κ, which is influenced by the jet physics, there is growing evidence that the magnetic field orientations in extragalactic radio jets often have a well-determined alignment to the local jet direction. In addition, the likelihood that any significant lens galaxy up to $z = 1$ can be now seen and have its redshift measured, enables "signature" positions of maximum $d\eta_G/d\theta$ along the background jet. These positions will be independent of any anomalies in $\kappa(\theta)$. As Figure 1 shows, the method is sensitive, in that the gravitational modulation of $\eta_G(\theta)$ operates on the derivative of $\delta(\theta)$. Also, any nongravitational distortion of the jet direction is effectively canceled out as long as κ is constant, or otherwise known.

The η_G effect is detectable over a large and optically observable range of lens redshift. It is also potentially applicable as a statistical test for dark matter halos over all redshift ranges out to approximately 2.5, the maximum distance to which a sufficient number of jet sources are currently visible and amenable to multifrequency radio polarimetric mapping. An important next stage in pursuing this method will be to obtain accurate observational determinations of $\kappa(\theta)$, possibly supported by computational MHD modeling of polarized jets, for a *low-redshift* group of radio jet objects. This sample, presumably minimally subject to gravitational lensing, would constitute a reference, or "null" sample, against which to search for η_G effects in jet probes at larger cosmological distances.

Financial support is acknowledged from the Natural Sciences and Engineering Council of Canada (NSERC) (PPK and CCD), and we thank the Directors and staff of the NRAO(VLA), NOAO (4 m telescope), and the Lick Observatory, respectively, for the provision of observing time and support. We thank Laura Carriere for her assistance with the data preparation, Donna Womble for reduction of the optical spectral data, and Ross Cohen for assistance with the Lick observations. E. M. Burbidge and V. T. Junkkarinen acknowledge financial support from NASA grant NAS5-29293.

REFERENCES

Bridle, A. H., Perley, R. A., & Henriksen, R. N. 1986, *AJ*, 92, 534
Clarke, D. A., Norman, M. L., & Burns, J. O. 1989, ApJ, 342, 700
Dyer, C. C., & Roeder, R. C. 1980, ApJ, 238, L67
———. 1981, ApJ, 249, 290
Gorenstein, M. V., Cohen, N. L., Shapiro, I. I., Rogers, A. E. E., Bonometti, R. J., Falco, E. E., Bartel, N., & Marcaide, J. M. 1988, ApJ, 334, 42
Greenfield, P. E., Roberts, D. H., & Burke, B. F. 1985, ApJ, 293, 370
Hewitt, J. N., Turner, E. L., Schneider, D. P., Burke, B. F., Langston, G. I., & Lawrence, C. R. 1988, Nature, 333, 537
Killeen, N., Bicknell, G. V., & Ekers, R. D. 1986, ApJ, 302, 306
King, I. R. 1972, ApJ, 174, L123
Kochanek, C. S., Blandford, R. D., Lawrence, C. R., & Narayan, R. 1989, MNRAS, 238, 43
Murray, C. A., Tucker, R. H., & Clements, E. D. 1971, RGO Bull., No. 162, p. 215
Perley, R. A., Bridle, A. H., & Willis, A. G. 1984, ApJS, 54, 291
Simard-Normandin, M., Kronberg, P. P., & Button, S. 1981, ApJS, 46, 239
Turner, E. L. 1987, in IAU Symposium 117, Dark Matter in the Universe, ed. J. Kormendy and G. R. Knapp (Dordrecht: Reidel), p. 227
Walsh, D., Carsell, R. F., & Weymann, R. J. 1979, Nature, 279, 736